J. Phys. B: At. Mol. Opt. Phys. 27 (1994) 3985–3992. Printed in the UK

Total and differential electron capture cross sections in B^{3+}/He collisions

M Gargaud†, F Fraija‡, M C Bacchus-Montabonel‡ and R McCarroll§

† Observatoire de l'Université Bordeaux I (URA 352 du CNRS), BP 89, F-33270 Floirac, France

‡ Laboratoire de Spectrométrie Ionique et Moléculaire (URA 171 du CNRS), Université Lyon I, Bâtiment 205, 43 Boulevard du 11 Novembre 1918, F-69622 Villeurbanne Cedex, France

§ Laboratoire de Dynamique Moléculaire et Atomique (URA 774 du CNRS), Université Pierre et Marie Curie, F-75252 Paris Cedex 05, France

Received 6 December 1993, in final form 13 June 1994

Abstract. Total, partial and differential cross sections for charge exchange collisions between B^{3+} and He have been determined in the 1 eV–10 keV energy range. The results are in excellent agreement with experiment and show that model potential calculations can be successfully adapted to the study of two-electron systems. The role of rotational coupling and the Stueckelberg oscillations of the differential cross sections are carefully examined.

1. Introduction

The B^{3+}/He system provides an ideal test case for the study of electron capture processes in collisions of multicharged ions with neutral atoms. It is relatively simple to describe theoretically since there are only two dominant electron capture channels (the ^2S and ^2P states of B^{2+}). On the other hand, both radial and rotational coupling mechanisms play an important role, so that a wide variety of dynamic effects can occur. Besides, the mass ratio is favourable for the experimental study of differential cross sections.

Total charge transfer cross sections were first measured by Zwally and Cable (1971) for ion energies in the 300 eV–30 keV energy range. Their results were fairly well reproduced by the theoretical calculations of Shipsey *et al* (1977) and Hansen *et al* (1992). The $^2S/^2P$ partial cross section ratio was measured by Matsumoto *et al* (1983) in the 1–3 keV energy range. Their results are comparable with the recent measurement of Roncin *et al* (1990) at an ion energy of 1.8 keV but both experiments give results which are greater than the theoretical predictions of Hansen *et al* by 60%. At 6 keV, the results of Matsumoto *et al* are more than a factor of 2 larger than the theoretical results.

However the comparison of total cross sections does not provide as much detail on the collision process as differential scattering cross sections. Very recently, the angular dependence of the ^2S and ^2P capture differential cross sections has been measured by Roncin *et al*. The differential cross sections at large scattering angles enable us to probe details of the collision dynamics which cannot be obtained from total cross sections (which are determined mainly by small angle contributions). Small angle scattering requires a good representation of long-range interactions, for which a two-centre expansion (Hansen *et al*) may be sufficient. But while an atomic expansion is adequate for a description of long-range collisions it is less satisfactory for close collisions at low energies, where rotational

0953-4075/94/173985+08$19.50

coupling plays an important role (Fraïja *et al* 1994). An adiabatic basis set is then more appropriate. To model the dynamics of the B^{3+}/He system over a wide angular range, we therefore require an accurate description both at short- and long-range interactions. This is not always easy to achieve by standard methods of quantum chemistry. In this work we explore the possibility of adapting model potential methods, which have proved very satisfactory for effective one-electron problems.

Although the B^{3+}/He system is basically a two-electron system (since the core electrons of B^{3+} play a passive role), the effect of electron correlation is only of primary importance in the initial channel correlated to the ^1S state of He; it is of secondary importance in the final channel. The non-adiabatic matrix elements between the different adiabatic states are dominated by the contributions from regions of space far from the vicinity of the nuclei. This situation was exploited by Grice and Herschbach (1974) for treating ionic–covalent configuration interaction in alkali-hydride and alkali-halide systems and was extended by Benmeuraiem *et al* (1987) to the Ar^{6+}/He system and by Gargaud *et al* (1989) to the O^{3+}/H system where correlation in the final channel is important. The most critical test of the method is for the Ar^{6+}/He system where this modified model potential method gives excellent agreement with experiment (Andersson *et al* 1989).

It is recalled that for the B^{3+}/He system, there are two dominant electron capture channels, leading to the formation of B^{2+} in the ^2S and ^2P states:

$$B^{3+}(1s^2) + He(1s^2) \rightarrow B^{2+}(1s^2 2p)^2P + He^+(1s) \tag{1}$$

$$\rightarrow B^{2+}(1s^2 2s)^2S + He^+(1s). \tag{2}$$

Four molecular states are implicated in the collisional process: the three Σ states (Σ_1 correlated to the ^2S exit channel, Σ_2 correlated to the ^2P exit channel and Σ_3 correlated to the entry channel) and the Π state correlated to the ^2P exit channel. These states are sufficient to describe the collision dynamics over a wide range of collision energies.

Atomic units will be used throughout except where otherwise stated.

2. Theory

The adaptation of the model potential technique to treat a system such as B^{3+}/He has been presented previously (Gargaud *et al* 1989) and only a few salient features of the practical application will be presented here. The first step is the generation of one-electron orbitals correlated to the 1s orbital of He in the entry channel and the 2s and 2p orbitals of B^{2+} in the exit channels using an effective two-centre model potential V_{eff}. The parameters which define V_{eff} are optimized so that the eigenvalues of the one-electron Hamiltonian correspond to the experimental ionization potentials. By analogy with quantum defect functions, these model orbitals do not necessarily give a good representation in the vicinity of the ionic cores, but they are satisfactory in those regions of space which contribute to the exchange integrals arising in electron capture processes. In the calculations the following form of V_{eff} was used.

$$V_{\text{eff}} = V_{B^{3+}}(r_a) + V_{He^+}(r_b) \tag{3}$$

where r_a and r_b are the electron coordinates with respect to the B^{3+} and He^+ ion cores respectively and

$$V_{B^{3+}}(r) = -r^{-1}[3 + (1 + c_1 r)e^{-d_1 r} + (1 + c_2 r)e^{-d_2 r}] \tag{4}$$

$$V_{He^+}(r) = -r^{-1}[1 + (1 + c_3 r)e^{-d_3 r}]. \tag{5}$$

The parameters of $V_{B^{3+}}(r)$ listed in table 1 have been optimized so that the eigenvalues of the model Hamiltonian

$$H_0 = T + V_{B^{3+}}(r) \tag{6}$$

where T is the kinetic energy operator, reproduce as well as possible the observed energy levels of B^{2+} ion. The optimization has been weighted to ensure that the asymptotic energies of those states which govern the charge transfer process are essentially exact (better than 0.0001%). The parameters c_3, d_3 of $V_{He^+}(r)$ are taken from the model potential already used by Opradolce *et al* (1983) in their study of the Ar^{6+}/He system: these are also listed in table 1.

Table 1. Model potential parameters of B^{3+} and He

$$V_{B^{3+}}(r) = -r^{-1}[3 + (1 + c_1 r)e^{-d_1 r} + (1 + c_2 r)e^{-d_2 r}]$$

$$V_{He^+}(r) = -r^{-1}[1 + (1 + (1 + c_3 r)e^{-d_3 r}].$$

	c_1	d_1	c_2	d_2	c_3	d_3
B^{3+}	1.0079	17.5963	15.0471	7.1230		
He^+					3.3636	1.6666

The eigenfunctions and eigenvalues of $(T + V_{eff})$ are calculated by standard variational techniques described by Valiron (1976) and Valiron *et al* (1979). The radial and rotational coupling matrix elements may then be computed directly. From the one-electron energies and non-adiabatic matrix elements, a set of diabatic orbitals is then generated according to the technique developed by Gargaud *et al* (1981). These diabatic orbitals are used to calculate the potential energies and matrix elements using the procedure of Grice and Herschbach. If one makes the reasonable approximation that the overlap of the 1s orbitals of He and He^+ is virtually unity, the procedure reduces to multiplying the off-diagonal one-electron diabatic matrix elements between the entry and exit channels by a factor of $\sqrt{2}$. An estimation of the precision of the technique can be gauged by rediagonalizing the diabatic matrix and comparing with *ab initio* calculations. Our adiabatic potentials, presented in figure 1, are in excellent agreement with *ab initio* calculations of Fraija *et al.*

In table 2, we compare our curve crossing parameters with the results of Fraija *et al* (1994) and Shipsey *et al.* For the inner crossing the agreement with Fraija *et al* is excellent while there is a 30% difference with Shipsey *et al.* On the other hand, for the outer crossing, the agreement with Shipsey *et al* is very satisfactory. However, there is a serious discrepancy with Fraija *et al* for the outer crossing, which appears to arise from the fact that their asymptotic energies are correctly described only up to 3×10^{-3} au, which is the order of magnitude of the separation energy of the outer crossing. Under these conditions, the calculations of Fraija *et al* cannot be expected to give a good description of long-distance crossings.

On the basis of this comparison of our model potential with the *ab initio* calculations of Fraija *et al*, it would therefore seem reasonable to adopt the model potential results for a study of the collision dynamics. There are several reasons. The first is that the asymptotic energy of all the interaction channels is exact. Secondly, our non-adiabatic interactions, in the vicinity of the outer crossing, may be expected to be more reliable than the *ab initio*

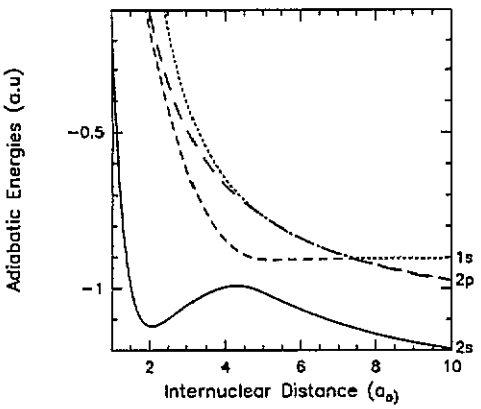

Figure 1. Adiabatic potential energy curves: ——, Σ_1, $B^{2+}(2s) + He^+(1s)$; – – –, Σ_2, $B^{2+}(2p) + He^+(1s)$; ----, Σ_3, $B^{3+}(1s^2) + He^+(1s^2)$; — — —, Π, $B^{2+}(2p) + He^+(1s)$.

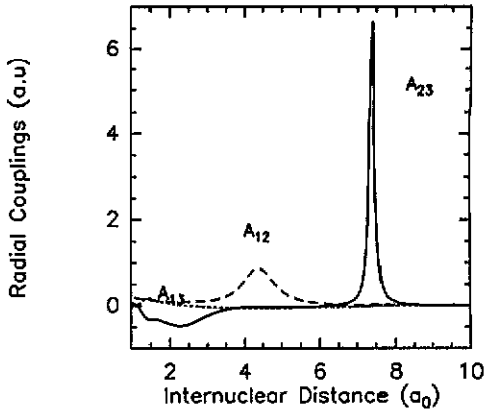

Figure 2. Radial coupling matrix elements: ——, $A_{23} = \langle\Sigma_2|\partial/\partial R|\Sigma_3\rangle$; – – –, $A_{12} = \langle\Sigma_1|\partial/\partial R|\Sigma_2\rangle$; ----, $A_{13} = \langle\Sigma_1|\partial/\partial R|\Sigma_3\rangle$.

Table 2. Comparison of our model potential curve crossings parameters with *ab initio* ones.

	Inner crossing		Outer crossing	
	R_x	ΔE	R_x	ΔE
Model potential	4.6	0.095	7.4	$3.0\ 10^{-3}$
Ab initio (Fraija *et al*)	4.4	0.100	7.0	$5.5\ 10^{-3}$
Ab initio (Shipsey *et al*)	4.7	0.070	7.4	$3.5\ 10^{-3}$

results. Thirdly, for the inner crossing parameters, where the *ab initio* calculations of Fraija *et al* are expected to be good, we note that these are also well described by the model potential technique.

We present in figures 2 and 3 the radial and rotational coupling matrix elements where allowance for translation effects has been made by the introduction of appropriate reaction coordinates (Gargaud *et al* 1987). In order to facilitate calculations down to eV energies, a quantum mechanical description of the collision dynamics has been adopted (Gargaud *et al* 1981).

3. Results and discussion

3.1. Total and partial cross sections

We present in figure 4 and table 3 our total and partial electron capture cross sections with and without the influence of rotational coupling. The agreement between the total experimental cross sections of Zwally and Cable and our theoretical ones is perfect in the 0.4–10 keV energy range and confirms the accuracy of our model potential method for the B^{3+}/He system. At lower energies there are unfortunately no absolute experimental data to compare with. We notice that rotational coupling effects are important for energies as low as 0.4 keV and nearly multiply the ^2P cross section by a factor of 2 for an energy of 2 keV.

In figures 5 and 6, we present the ^2S and ^2P electron capture transition amplitudes as a function of impact parameter for an energy of 6 keV, where rotational coupling is of major

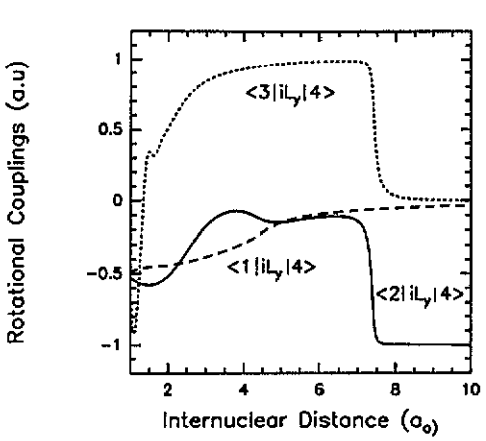

Figure 3. Rotational coupling matrix elements: – – –, $\langle\Sigma_1|iL_y|\Pi\rangle$; ——, $\langle\Sigma_2|iL_y|\Pi\rangle$; – – –, $\langle\Sigma_3|iL_y|\Pi\rangle$.

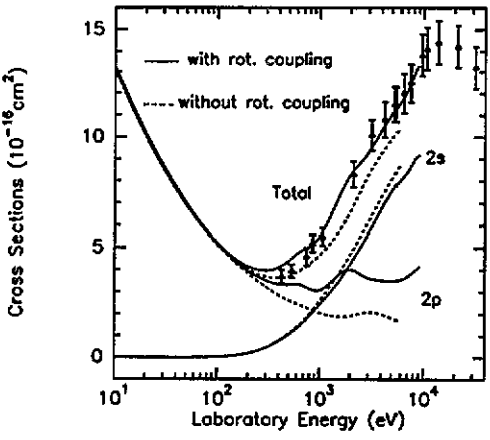

Figure 4. Total and partial charge transfer cross sections (10^{-16} cm^2) as a function of ion energy (eV): ——, with rotational coupling; – – –, without rotational coupling; ▲, experiment (Zwally and Cable).

Table 3. Total and partial cross sections (10^{-16} cm^2) as a function of ion energy (eV).

E (eV)	2s	$2p_\Sigma$	$2p_\Pi$	2p	Total
1.0	0.00	24.83	1.51	26.34	26.34
5.1	0.00	12.79	3.81	16.6	16.6
10.3	0.00	8.25	4.88	13.13	13.13
51.0	0.00	2.92	4.04	6.96	6.96
102	0.03	2.04	4.68	5.15	5.18
306	0.48	1.28	2.22	3.50	3.97
510	1.09	1 17	2.16	3.34	4.42
612	1.38	1.14	2.23	3.37	4.75
963	2.34	0.84	2.21	3.06	5.40
1500	3.38	1.09	2.52	3.61	7.00
1800	3.91	1.30	2.68	3.98	7.89
2167	4.53	1.20	2.78	3.98	8.51
2737	5.34	0.98	2.73	3.71	9.05
3851	6.63	0.93	2.61	3.54	10.17
6018	8.05	0.82	2.73	3.55	11.60
7137	8.46	0.94	2.79	3.73	12.19
8157	8.95	1.09	2.86	3.95	12.90
9177	9.16	1.19	2.96	4.15	13.31

importance. The ^{2}P electron capture transition amplitude exhibits two maxima, one for an impact parameter of 1.6 a_0, the other for an impact parameter of 5.7 a_0, corresponding respectively to capture via the Σ_2–Π crossing around $R = 2$ a_0 and the outer Σ_2–Σ_3 crossing around $R = 7.4$ a_0. It is clear from figure 6 that at very short internuclear distances rotational coupling is much more important than radial coupling. At the outer crossing, radial coupling is dominant. The ^{2}S capture transition amplitude is maximum at an impact parameter of about 3.3 a_0; in this case, radial coupling at the inner Σ_1–Σ_2 avoided crossing is the dominant capture mechanism.

In figure 7 we compare our theoretical total cross sections with the *ab initio* calculations of Shipsey *et al* and the two-centre atomic orbital expansion of Hansen *et al*. For energies

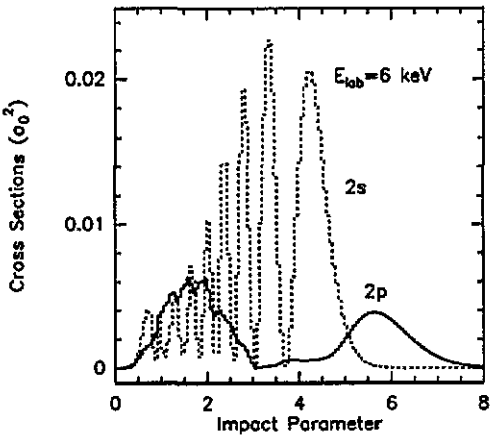

Figure 5. ^2S and ^2P electron capture transition amplitudes as a function of impact parameter for an energy of 6 keV: ——, ^2P contribution; - - - -, ^2S contribution.

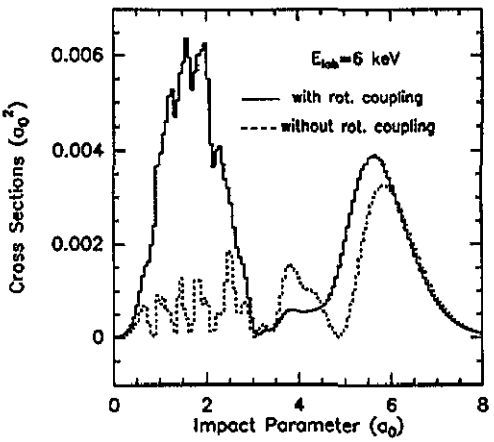

Figure 6. ^2P electron capture transition amplitude as a function of impact parameter for an energy of 6 keV: ——, with rotational coupling; – – –, without rotational coupling.

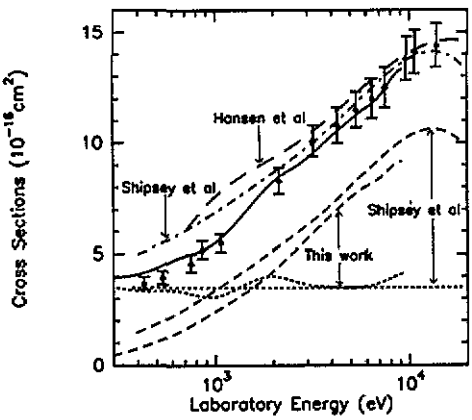

Figure 7. Total and partial cross sections (10^{-16} cm^2): - - - -, ^2S (this work and Shipsey *et al*); – – –, ^2P (this work and Shipsey *et al*); ——, total (this work); — — —, total (Hansen *et al*); — · —, total (Shipsey *et al*); ▲, experiment (Zwally and Cable).

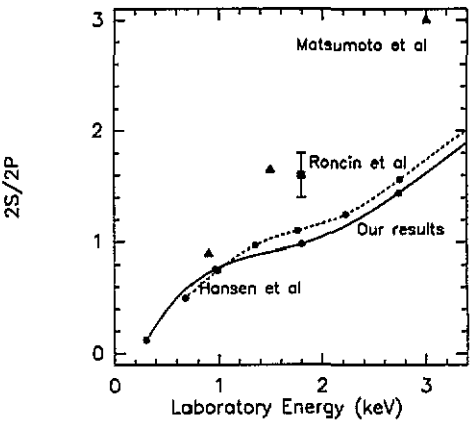

Figure 8. $^2S/^2P$ cross section ratio as a function of energy: ——, this work; – – –, Hansen *et al*; ▮, experiment (Roncin *et al*); ▲, experiment (Matsumoto *et al*).

exceeding 3 keV, all the theoretical models are in good agreement. At lower energies, our results are in better agreement with experiment.

In figure 8, we compare our $^2S/^2P$ cross section ratio in the energy range 0.3–3.4 keV with the theoretical values of Hansen *et al* and the measured values of Roncin *et al* and Matsumoto *et al*. Although the agreement between both theories is excellent, there is a considerable divergence from the experimental results. We believe that it is difficult to reconcile this experimental ratio with theory. A possible explanation is proposed in the following section.

Table 4. $^2S/^2P$ cross section ratio as a function of ion energy and acceptance angle.

	θ_M (deg)								
E_{lab} (keV)	0.57	1.14	2.29	3.44	4.58	5.72	6.87	8.02	9.17
0.31	0.10	0.06	0.07	0.07	0.08	0.08	0.09	0.10	0.11
0.96	0.69	0.61	0.80	0.86	0.82	0.79	0.77	0.76	0.76
1.80	1.30	1.48	1.12	1.04	0.99	0.99	0.99	0.98	0.98
2.74	2.23	1.92	1.49	1.43	1.44	1.44	1.44	1.44	1.44
6.02	2.83	2.36	2.29	2.29	2.29	2.29	2.29	2.29	2.29

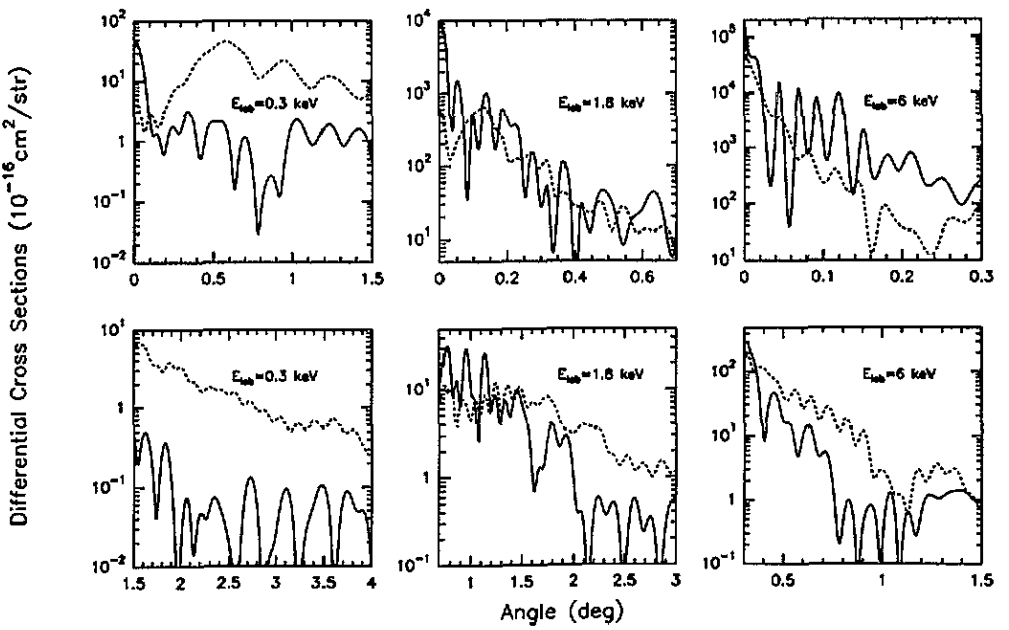

Figure 9. Differential cross sections (10^{-16} cm^2 sr^{-1}) as a function of scattering angle for ion energies of 0.3 keV, 1.8 keV, 6 keV: ——, ^2S; – – –, ^2P.

3.2. Differential cross sections

The differential cross sections have been calculated from the S-matrix elements using the method described by Andersson *et al* (1991). We present in figure 9 the ^2S and ^2P differential cross sections. For $E = 0.3$ keV the ^2S channel is dominant at very small angles ($\theta \leqslant 0.15°$). At larger angles the ^2P capture prevails. For $E = 1.8$ keV the ^2S is still dominant at very small angles ($\theta \leqslant 0.07°$), but with increasing angle capture to the ^2S and ^2P channels is evenly divided between the two up to $\theta = 1.5°$. For $\theta > 1.5°$ the ^2P channel prevails. For $E = 6$ keV the ^2S channel is dominant, not only at very small angles but over the angular range $0 < \theta < 0.5°$, but for $\theta \geqslant 0.5°$ the ^2P channel prevails. These results compare very favourably with the experiment of Roncin *et al* at an energy of 1.8 keV. Since the results of Roncin *et al* are not in absolute units, it has not been possible to represent them on the same figure.

The oscillations observed in the differential cross sections are of Stueckelberg type: for a given energy the angular separation between two maxima is constant ($\Delta\theta$ is of the order

of 0.06° for $E = 1.8$ keV, $\Delta\theta$ of the order of 0.03° for $E = 6$ keV). This separation $\Delta\theta$ is inversely proportional to $\sqrt{E}$.

The results of figure 9 indicate that capture to the ^{2}P channel always dominates at large scattering angles. This implies that if the angular acceptance of the B^{2+} detector were limited there would be a tendency for the experimental $^2S/^2P$ cross section ratio to overestimate the true value. An illustration of this effect is given in table 4, where we present the $^2S/^2P$ cross section ratio as a function of the acceptance angle of the detector. The effect is obviously most spectacular at low energies but even at an energy of 1.8 keV, the ratio for an acceptance angle of 1° exceeds the true value by about 50%. We propose this effect could explain the discrepancy between theory and experiment observed in figure 8.

4. Conclusion

Our results confirm that the model potential method can be successfully adapted to treat an effective two-electron system, such as B^{3+}/He where the ionic core remains passive and electron correlation is only of real influence in the target atom. Model potential methods are particularly advantageous in describing accurately long- and intermediate-range interactions which control the collision dynamics.

Comparison with total and differential cross sections indicates that our theoretical predictions for electron capture processes are remarkably accurate over a wide range of energies and scattering angles.

References

Andersson L R, Gargaud M, McCarroll R 1991 *J. Phys. B: At. Mol. Opt. Phys.* **24** 2073

Andersson L R, Pedersen J O P, Bárány A, Bangsgaard J P and Hvelplund P 1989 *J. Phys. B: At. Mol. Opt. Phys.* **22** 1603

Benmeuraiem L, McCarroll R and Opradolce L 1987 *Proc. 15th Int. Conf. on Physics of Electronic and Atomic Collisions* ed J Geddes, H B Gilbody, A E Kingston, C J Latimer and H R J Walters (Amsterdam: North-Holland) Abstracts p 557

Fraija F, Bacchus-Montabonel M C and Gargaud M 1994 *Z. Phys.* D **29** 179

Gargaud M, Hansen J, McCarroll R and Valiron P 1981 *J. Phys. B: At. Mol. Phys.* **14** 2259

Gargaud M, McCarroll R and Opradolce L 1989 *Astron. Astrophys.* **208** 251

Gargaud M, McCarroll R and Valiron P 1987 *J. Phys. B: At. Mol. Phys.* **20** 1555

Grice R and Herschbach D R 1974 *Mol. Phys.* **27** 159

Matsumoto A, Iwai T, Kaneko Y, Kimura M, Kobayashi N, Ohtani S, Okuno K, Takagi S, Tawara H and Tsurubuchi S 1983 *J. Phys. Soc. Japan* **52** 3291

Opradolce L, Valiron P and McCarroll R 1983 *J. Phys. B: At. Mol. Phys.* **16** 2017

Roncin P, Adjouri C, Gaboriaud M N, Guillemot L, Barat M and Andersen N 1990 *Phys. Rev.* A **65** 3261

Shipsey E J, Browne J C and Olson R E 1977 *Phys. Rev.* A **15** 2166

Valiron P 1976 *3rd Cycle Thesis* Université de Bordeaux

Valiron P, Gayet R, McCarroll R, Masnou-Seeuws F and Philippe M 1979 *J. Phys. B: At. Mol. Phys.* **12** 53

Zwally H J and Cable P G 1971 *Phys. Rev.* A **4** 2301